Journal of Biomedical Optics

BiomedicalOptics.SPIEDigitalLibrary.org

Noncontact imaging of burn depth and extent in a porcine model using spatial frequency domain imaging

Amaan Mazhar
Steve Saggese
Alonda C. Pollins
Nancy L. Cardwell
Lillian Nanney
David J. Cuccia

SPIE.

Noncontact imaging of burn depth and extent in a porcine model using spatial frequency domain imaging

Amaan Mazhar,[a,*] Steve Saggese,[a] Alonda C. Pollins,[b] Nancy L. Cardwell,[b] Lillian Nanney,[b] and David J. Cuccia[a]
[a]Modulated Imaging Inc., Beckman Laser Institute Photonic Incubator, 1002 Health Sciences Road, Irvine, California 92617, United States
[b]Vanderbilt University, Department of Plastic Surgery, Cell and Developmental Biology, Nashville, Tennessee 37232, United States

Abstract. The standard of care for clinical assessment of burn severity and extent lacks a quantitative measurement. In this work, spatial frequency domain imaging (SFDI) was used to measure 48 thermal burns of graded severity (superficial partial, deep partial, and full thickness) in a porcine model. Functional (total hemoglobin and tissue oxygen saturation) and structural parameters (tissue scattering) derived from the SFDI measurements were monitored over 72 h for each burn type and compared to gold standard histological measurements of burn depth. Tissue oxygen saturation (stO_2) and total hemoglobin (ctHbT) differentiated superficial partial thickness burns from more severe burn types after 2 and 72 h, respectively ($p < 0.01$), but were unable to differentiate deep partial from full thickness wounds in the first 72 h. Tissue scattering parameters separated superficial burns from all burn types immediately after injury ($p < 0.01$), and separated all three burn types from each other after 24 h ($p < 0.01$). Tissue scattering parameters also showed a strong negative correlation to histological burn depth as measured by vimentin immunostain ($r^2 > 0.89$). These results show promise for the use of SFDI-derived tissue scattering as a correlation to burn depth and the potential to assess burn depth via a combination of SFDI functional and structural parameters. [DOI: 10.1117/1.JBO.19.8.086019]

Keywords: spatial frequency domain imaging; burn wound assessment; optical properties; tissue scattering; multispectral imaging.

Paper 140354R received Jun. 5, 2014; revised manuscript received Jul. 23, 2014; accepted for publication Jul. 28, 2014; published online Aug. 22, 2014.

1 Introduction

An estimated 11 million people suffer from burn injuries globally.[1] In the United States, this number is estimated to be 450,000, of which 40,000 injuries are severe enough to cause hospitalization.[2] An accurate assessment of burn depth-a measure for tissue viability postinjury-is essential for proper burn treatment. Thermal burn injuries are clinically classified according to the depth of the injury as superficial, superficial partial thickness, deep partial thickness, or full thickness. Superficial and full-thickness burns are readily diagnosed by expert clinicians due to the distinct nature of dermal tissue status. The true clinical challenge lies in determining the outcome of partial thickness injuries where the dermal layer is partially damaged. In these injuries, re-epithelialization can occur if adequate vasculature is present. However, the vasculature is often compromised too much and re-epithelialization cannot occur making excision and grafting necessary. In these cases, clinical determination may occur days after the initial injury due to the evolution of the wound, leaving the patient susceptible to infection, increased scarring, and pain.

Despite advances in medical technologies, the primary method for burn depth assessment remains a subjective clinical evaluation. The accuracy of clinical assessment depends entirely on the skill of the clinician and studies have shown that the clinician diagnosis matches the outcome for somewhere between 50% and 65% of the cases.[3–6] Mismanaged burn treatment can have severe physical (infection, pain, and mortality), psychological (scarring and trauma), and financial (longer hospital stays and medication) consequences on the patient and the healthcare system. A quantitative and standardized tool to assess burn depth in the acute phases of care could potentially improve the accuracy and precision of assessing burn severity and improve the overall cost effectiveness of burn wound care. To address this issue, we present pilot data acquired in a porcine graded burn severity model using a prototype optical imaging system (based on spatial frequency domain imaging).

Many histological methods have been proposed as gold standards to measure the burn depth based on functional and structural integrity of the tissue.[5] For this work, we used vimentin-an immunostain that identifies highly differentiating cells-to measure the burn depth by evaluating the functional status of tissue. Vimentin has been successfully demonstrated to accurately identify burn depth and highlight the evolving nature of the wound.[7] Second, we used Masson's Trichrome stain to evaluate the structural integrity of the collagen fibrils in each type of burn wound. Although histological analysis is a tremendous tool for validation, clinical translation of histology can be limited because obtaining samples through punch biopsies are invasive, painful, single time snapshots, and are limited to small regional areas.

Many noninvasive technologies have been proposed for quantitative assessment of burn depth. These technologies include but are not limited to laser Doppler imaging (LDI), multi-spectral imaging,[8] intravital imaging,[9,10] terahertz imaging,[11] polarization sensitive optical coherence tomography

*Address all correspondence to: Amaan Mazhar, E-mail: amaan.mazhar@modulatedimaging.com

(psOCT),[12,13] and reflectance microscopy.[14] There are a number of benefits and disadvantages for these technologies, which have been nicely summarized in review articles.[15,16] The utility and adoption of these technologies are often judged by performance (i.e., precision, specificity, sensitivity, and validation), ease of use (i.e., speed, mobility, patient comfort, ease of interpretation, duration, and learning curve), costs (i.e., machine maintenance, personnel, and training), and suitability for different types of burn management styles (i.e., aggressive early excisions and grafts versus wait and see). Many of the technologies mentioned above fall short in one or more categories; however, LDI meets many of these requirements and historically has achieved the most adoption within burn units. LDI uses light to indirectly assess tissue health by noninvasively mapping skin and subsurface blood flow. Studies have shown that blow flow is strongly correlated to the healing time of burn wounds 72 h after the initial burn wound based on the premise that blood flow is maintained in damaged tissue.[17] This diagnosis time is an improvement over traditional care as surgeons have opted for earlier excision based on LDI and this has potentially reduced hospitalization time.[18] Despite the success of LDI, scan times for LDI over typical fields of view (>200 cm^2) are slow (~minutes), limiting measurements of large areas due to motion artifacts. LDI data also have been shown to vary between patients/studies and also can be affected by eschar and edema due to the change in tissue optical properties.[19,20]

Near-infrared (NIR) spectroscopy has shown similar promise in measuring tissue functionality for burn wound assessment. The functional status of a burn has been measured by extracting the hemoglobin levels, tissue oxygen saturation (stO_2), and edema using wavelength-dependent light transport models.[21,22] This has been done both in the context of point spectroscopy and imaging. In this work, we present an extension of these NIR spectroscopy concepts to quantitative, wide-field imaging using a method called spatial frequency domain imaging (SFDI). SFDI is a noncontact optical imaging technology that has the capability for spatially resolving optical absorption and scattering parameters at each wavelength.[23,24] By separating and quantifying the multispectral absorption and scattering optical properties, SFDI can directly account for photon path length, and thus remove the crosstalk in reflectivity changes resulting from physically distinct contrast mechanisms (i.e., differentiate chromophore absorption versus tissue scattering from structural components such as collagen). Therefore, SFDI has the potential for a more direct assessment of tissue functional and structural state. Moreover, SFDI can spatially resolve these properties with modest resolution (<1 mm) over large fields of view (>10 s of cm), allowing for the visualization of the lateral extent of a wound. SFDI has been demonstrated in several applications including skin flaps,[25–27] port-wine stains,[28] and cancer.[29] In the area of burns, SFDI has been demonstrated to track acute changes in tissue chromophores for different burn severities[30] and to identify the onset of infection due to burn injury.[31]

2 Materials and Methods

2.1 *Spatial Frequency Domain Imaging Method*

SFDI is practiced by projecting spatially modulated illumination (typically periodic) patterns of various spatial frequencies over a large (many cm^2) area of a sample and capturing the reflected images with a camera.[23,24] The demodulation of these spatially modulated waves characterizes the sample modulation transfer function (MTF), which encodes the optical property information-absorption and reduced scattering. Accelerated Monte Carlo-based analysis of MTF data results in two-dimensional maps of the quantitative absorption (μ_a) and reduced scattering (μ_s') optical properties via the least-squares fitting or look-up table approaches.[23,32] Height maps are calculated using the spatially varying phase to accommodate the measurement of curved surfaces in analysis.[33] When spectroscopy is desired, the SFDI measurement is repeated at multiple wavelengths, which results in a sparse spectrum of μ_a, and μ_s' optical properties versus a wavelength at each pixel. Recovered absorption data at an optimal combination of wavelengths can be used to fit for functional chromophore concentrations (Fig. 1), such as deoxy-hemoglobin (ctHHb), oxy-hemoglobin (ctO_2Hb), hemoglobin (ctHbT), tissue oxygen saturation, and water (ctH_2O).[34] The wavelength-dependent reduced scattering coefficient at each wavelength can be fit to the power-law decay:

$$\mu_s' = A\left(\frac{\lambda}{\lambda_o}\right)^{-b}. \quad (1)$$

In this equation, A is proportional to the density of the scattering particles and b is related to the average scatter size (collagen, nuclei, and mitochondria).[35] In skin, the collagen fibrils in the dermis are major contributors to the scattering signal.[36]

2.2 *Spatial Frequency Domain Imaging Instrumentation*

The SFDI device used in this study was a compact, clinic friendly, light emitting diode (LED)-based system developed by Modulated Imaging Incorporated (MI Inc., Irvine, California) for research purposes [Figs. 1(a) and 1(b)]. This general purpose SFDI system was designed for rapid imaging of a 15 × 20 cm

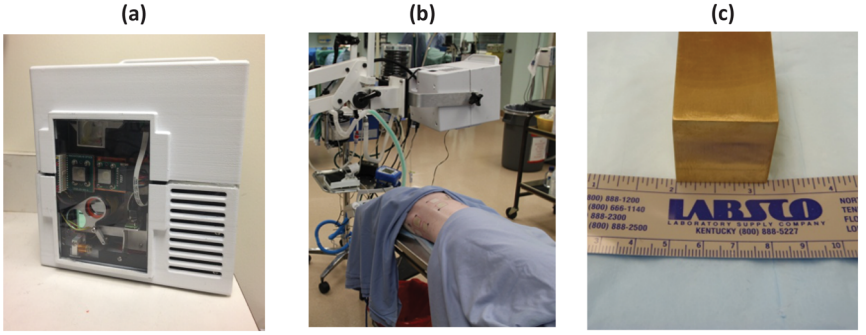

Fig. 1 (a) Prototype imaging head, (b) imaging head taking data on portable cart, (c) brass burning tool.

field of view (FOV. Microcontroller electronics synchronized LED pulses with a digital micromirror device projection (Discovery 3000 w/0.7" XGA LVDS DMD, Texas Instruments Inc., Dallas, Texas) and camera acquisition (LU160m, Lumenera Corp., Ottawa, Canada) to enable rapid image sequence and capture (~5 ms integration times) for all spatial patterns and illumination wavelengths. A custom thermoelectric board is used to maintain LED stability and temperature. Polarizers are placed in cross-polarized orientation after the source and before the detector to reject specularly reflected light from the tissue surface. The system simultaneously collected color photography with calibrated, color-balanced white light illumination, which enabled a standardized method of comparing SFDI results with visual clinical impressions. Data were acquired using 10 wavelengths in the system (400 to 850 nm) and at five spatial frequencies (0 to 0.2 mm^{-1}). Height profile data at a single spatial frequency ($f_x = 0.15$) were also acquired to correct for height and angle-dependent reflectance changes. Data were analyzed by fitting for optical properties at each wavelength, using a homogenous Monte Carlo SFD light transport model. A nonlinear least-squares fit to tissue reflectance was carried out for each pixel and wavelength using all five frequencies via a Levenberg–Marquardt algorithm implemented in C# software, where the forward model was based on precomputed Monte Carlo simulations. Subsequently, a linear least-squares fit was applied to transform the absorption maps to a tissue chromophore concentration. On a quad-core 3.3 GHz computer (Intel Core i5), optical property and tissue chromophore recovery took ~54 s per dataset (or 14 μs/pixel). For this analysis, chromophores were fit using only the NIR data (650 to 850 nm). Scatter cross-section and wavelength-dependent parameters were fit using full visible and NIR data.

2.3 *Preclinical Burn Model*

All animal work was performed under Vanderbilt Institutional Animal Care and Use Committee (IACUC) and United States Army Animal Care and Use Review Office (ACURO) approved study protocols. Yorkshire pigs (mean weight = 65 lb) were anesthetized with an intramuscular injection of ketamine plus xylazine. The dorsal surface of the pig was clipped, shaved, and washed with mild soap and disinfected with povidone-iodine. Contact thermal burns were created on the pig skin using a square brass rod [Fig. 1(c)] heated to 100°C in boiling water.[37,38] The burn wounds in this study were imparted on the pig using a "reverse time course" model. On day 0, a total of six burn injuries were imparted on an animal; two wounds of each severity on either side of the animal (Fig. 2). The severity of the injury was controlled by altering the contact time; a 12 s contact time led to a superficial partial thickness thermal injury (green), 24 s to a deep partial thickness injury (yellow), and 75 s to a full thickness injury (red). Three wounds were placed on either side (six total) of the animal during a single session with one of each burn type located on a defined grid on the animal. Six additional burns (two of each severity) were imparted in a similar fashion for each subsequent day to achieve the time points of 24, 48, and 72 h. Burns made on the final day were allowed to progress for 2 h after each wound was introduced, including those of the final day. Thus, multiple burn wounds at all four desired time points (2, 24, 48, 72 h postinjury) could be harvested from the animal on the final day. Burns were placed on either side of the animals and a total of two animals were used in this study in order to obtain a total of 48 wounds. The "reverse time-course" model eliminates the need for intermediate punch biopsies at each time point, reducing the risk of wound complications due to biopsy caused infection and inflammation.[37,38] Additional SFDI measurements were taken immediately postburn and after 1 h, but there was no histology to represent this time point. SFDI data were collected using the system described above (Fig. 1) for each measurement time point. Histology procedures included two immunostains such as vimentin and Masson's Trichrome. Vimentin is an immunomarker that identifies viable mesenchymal cells in burned skin. These cells represent the sites of activity where the wound still has viable cells beginning the

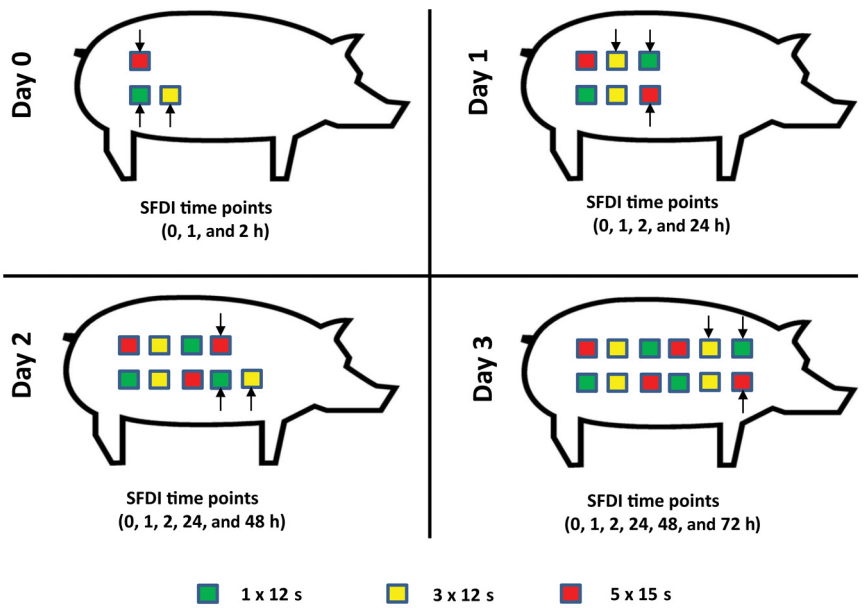

Fig. 2 Diagram of reverse time course wound model employed in this study. Colors correlate to burn severity and arrows indicate new wounds. This sequence was repeated on both sides of the animal. After day 3, the animal was sacrificed and the tissue was salvaged for histology. Histology time points included $t = 2$, 24, 48, and 72 h.

wound healing steps. In a burn wound, a visible junction between positively stained cells and unstained cells can be used to assess the burn depth in a pig burn.[7] Masson's trichrome was used as a way to look at the morphology of the dermal collagen, which is a key contributor to the SFDI scattering signals.

3 Results

3.1 *Optical Property Maps of Burn Wounds*

A total of 48 wounds were analyzed for this study, 16 of each severity (superficial partial, deep partial, and full thickness). The representative color and SFDI images of each wound type highlight the diverse nature of contrast for different burn depths. Color images captured the visual evolution of the burn wound over 72 h. As shown in Fig. 3(a), deep partial thickness and full thickness burns are nearly indistinguishable over the first 48 h to the visible eye. In Fig. 3(b), a calibrated planar (flood illumination) diffuse reflectance at a single NIR wavelength (658 nm) shows some graded contrast for each wound type over the course of the first 48 to 72 h. The wavelength of 658 nm was chosen as a representative in the middle of the visible and NIR range. We observed that the trends in contrast were similar at all wavelengths (see Sec. 3.2, Fig. 5 and related discussion for quantitative region of interest (ROI) values across all wavelengths). Separating reflectivity into absorption [Fig. 3(c)] and scattering [Fig. 3(d)] components using SFDI reveals that scattering appears to have earlier time sensitivity to burn severity that remained constant over 72 h. In the case of the most superficial burns, scattering values increase compared to surrounding normal tissue, but decrease in the case of the two more severe burns [Fig. 3(d)]. Multiwavelength SFDI analysis yielded NIR absorption spectra at each pixel that can be used to measure the tissue functionality, resulting in maps of stO_2 [Fig. 3(e)] and tissue hemoglobin (images not shown for brevity but mean values are presented in Fig. 6). stO_2 maps show a decrease in tissue saturation at early time points for the two most severe wounds. After 24 h, stO_2 for the deep partial wound levels out while full thickness burns continue to decline [Fig. 3(e)]. As described in Sec. 2.1, the wavelength dependence of the tissue reduced scattering coefficient can be quantitatively modeled as a polydisperse collection of Mie scattering sphere particles, where the scattering coefficient is related to the size and density of the scattering objects in tissue. At each pixel,

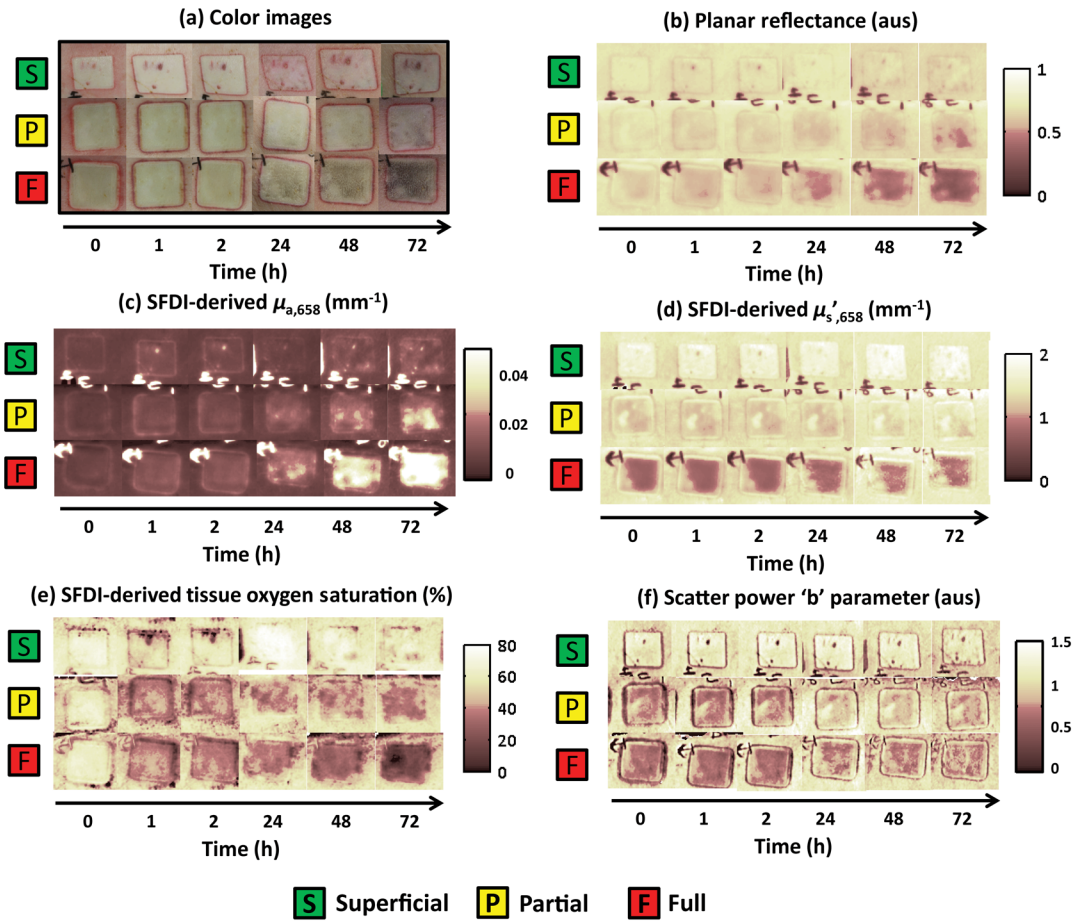

Fig. 3 Derived SFDI maps for three burn severities highlighted the potential to monitor wounds over time. (a) Color images showed the similarity between wound types during acute stages of the injury. Single wavelength (b) reflectance images and (c) absorption (658 nm) differentiated among all three burn types after 72 h, (d) single wavelength scattering images showed differential contrast immediately postburn and was significant for each burn type after 24 h, multiwavelength absorption was used to quantify (e) tissue oxygen saturation (stO_2) and differentiated between burn types after 72 h. Finally, multiwavelength scattering was used to fit for the "b parameter" which showed differential contrast after 24 h.

wavelength-dependent scattering data were fitted to a power law Eq. (1) to derive A (scattering cross section) and b (wavelength dependence) parameters using a center wavelength $\lambda_o = 800$. As shown in Fig. 3(f), wavelength-dependent scatter power parameter (b) slightly increases compared to the surrounding normal tissue for superficial wounds and conversely decreases for the two more severe wounds. This result was consistent with the scattering results presented above.

3.2 *Quantitative Structural and Functional Tracking of Burned Tissue*

To quantify the differential contrast among superficial partial, deep partial, and full thickness burns across all the burns, an ROI was chosen for each wound and the mean values for each recovered parameter were tracked over time. The ROI chosen was a 50×50 pixel area ($\sim 15 \times 15$ mm) in the middle of the wound. If there was a blister in the wound, this area was avoided in both histology and SFDI ROI selection. This analysis resulted in four mean ROI values per wound severity at each time point. A one-tailed paired *t*-test was performed for all mean ROI values at each time point to determine the significance for each recovered parameter. Single wavelength reflectance [Fig. 4(a)] at 658 nm differentiated among all three burn types after 72 h ($p < 0.01$). Figure 4(a) shows that the reflectance values for superficial wounds are significantly different from those of the two most severe wounds after the initial burn injury. Figure 4(b) shows that by separating tissue reflectance into absorption and scattering parameters, 658 nm absorption does not differentiate any of the burn severities from each other except for the case of the most severe burn [Fig. 4(b)]. In this case, the most severe burn has a significant increase in absorption compared to the other wounds after 72 h ($p < 0.01$). In contrast, Fig. 4(c) demonstrates that scattering values differentiate between all wound types 24 h ($p < 0.01$) after the injury as opposed to 72 h. These results suggest that the sensitivity observed in single wavelength reflectance was likely due to scattering changes. Interestingly, scattering values clearly identified superficial partial thickness wounds from the deep partial and full thickness immediately postburn independent of the evolving functional status of the tissue. As we discuss below, this differentiation could be an early indicator of outcome and, hence, treatment plan.

Other wavelengths show similar trends as those derived from the 658-nm optical properties. In Fig. 5, we plot the mean multiwavelength absorption and scattering [Figs. 5(a) and 5(b)] spectra at 24 h to show the wavelength-dependent sensitivity to burn severity, as well as the improved sensitivity of the scattering spectrum to burn injury severity as compared to that of the absorption spectrum. Wavelength-dependent absorption does not differentiate the three wound severities from each other at any wavelength after 24 h. However, recovered scattering values at four wavelengths (470, 658, 690, and 730 nm) differentiated all burn types from each other ($p < 0.01$). Data acquired at 400 nm were excluded during analysis due to concerns about tissue autofluorescence.[39] Multiwavelength absorption data were fit to tissue chromophores (ctHbT, stO_2) to describe the functional status of the tissue, and scattering was fit to describe the structural status of the tissue (collagen fibril diameter, density). Tissue chromophore values were able to differentiate between superficial burns and the deep partial/full thickness burns in the first 72 h ($p < 0.01$). stO_2 values differentiate the superficial wounds ($p < 0.01$) prior to total blood volume values [Figs. 6(a) and 6(b)]. It is important to note that these functional parameters were not able to differentiate between the deep partial thickness and full thickness wounds in the first 72 h, possibly due to uncertainty in the final wound outcome. Wavelength-dependent scattering parameters showed a similar sensitivity to burn severity as that of a single wavelength scattering [Figs. 7(a) and 7(b)]. All wounds were separable ($p < 0.01$) after 24 h for both A and b scattering-derived parameters. Superficial burns were distinguishable from the other severities immediately after the injury.

3.3 *Spatial Frequency Domain Imaging Scattering Parameters Correlated with Histological Burn Depth*

Tissue histology was used as a gold standard metric of burn depth to validate the correlation between SFDI scattering values

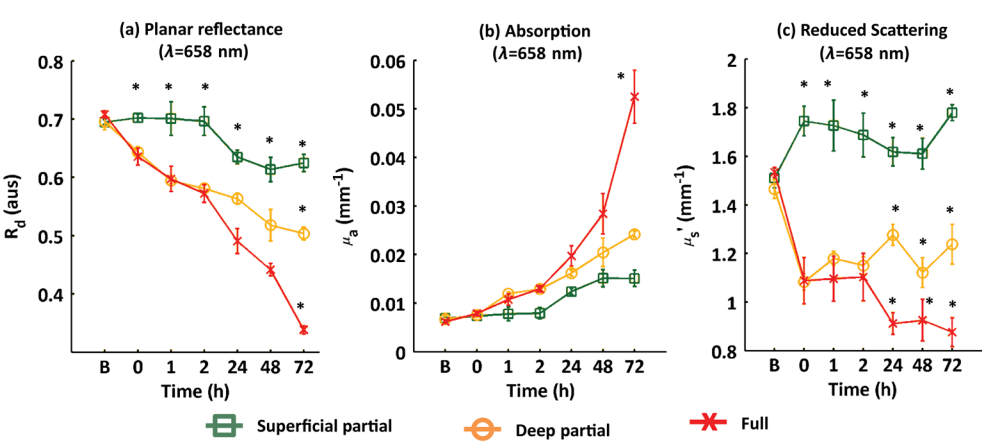

Fig. 4 Region of interest (ROI) time course data for three different burn severities show that single wavelength (a) planar reflectance, SFDI-derived (b) absorption (μ_a) and (c) reduced scattering (e.g., μ_s') measures are sensitive to burn depth. Time points with asterisk represent burn types that are significantly different compared to other burn types (p<0.01). Reflectance was significantly different for all three burn types after 72 h. Absorption was unable to differentiate among all three burn types after the first 72 h. In contrast, recovered scattering was significantly different for all three burn types after 24 h. Error bars represent the standard error between animals.

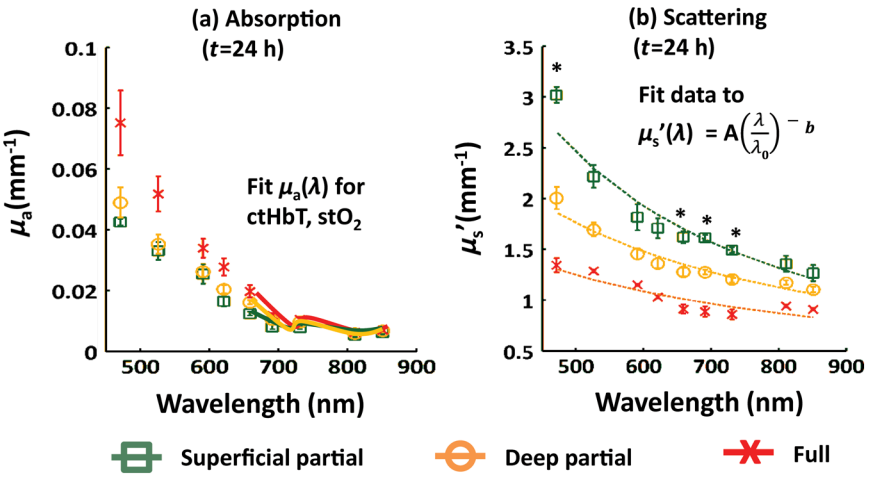

Fig. 5 Average wavelength dependent (a) absorption and (b) reduced scattering parameters 24 h postinjury for all three burn types. Near-infrared (NIR) absorption values were used to fit for tissue physiological parameters (tissue hemoglobin, tissue oxygen saturation) and visible/NIR scattering values were used to fit for power law. Error bars represent the standard error between animals.

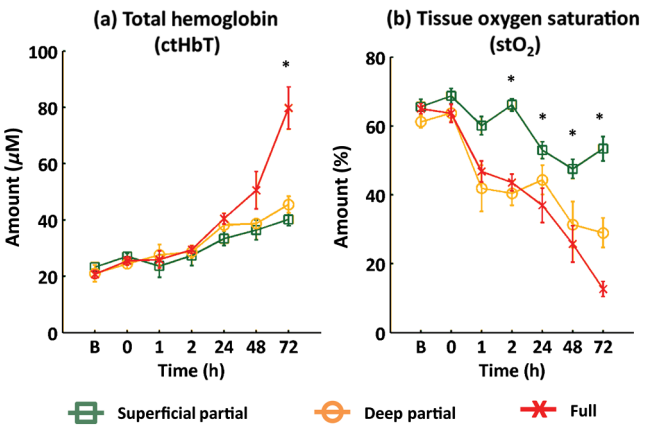

Fig. 6 Tissue functional parameters were fit using NIR absorption values. Recovered values for (a) tissue-level hemoglobin were significantly different for full-thickness burns only after 72 h. Recovered values for (b) tissue oxygen saturation (stO_2) were significantly different for superficial partial thickness wounds within 2 h. Error bars represent the standard error for all animals.

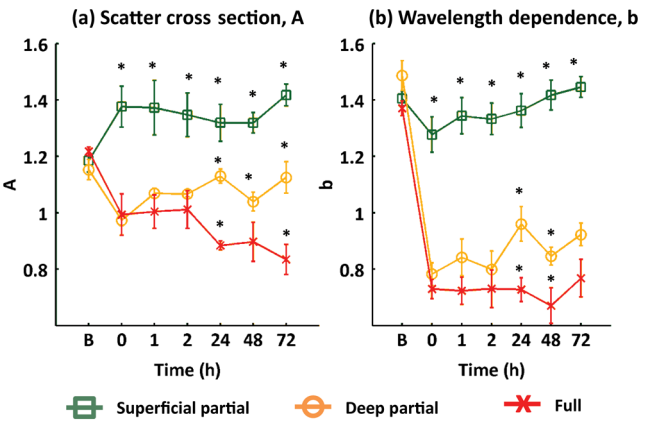

Fig. 7 Wavelength-dependent scattering values for each burn type and at each time point were fit to a power law to approximate (a) scattering cross section and (b) wavelength-dependent parameter. Superficial partial thickness burns were immediately identifiable postburn from other burn types. However, deep partial and full thickness burns only became separable after 24 h. Error bars represent the standard error for all animals.

and burn severity. The vimentin immunostain was used to determine the burn depth at each time point (2, 24, 48, and 72 h) and for each type of burn (superficial partial, deep partial, and full). For this study, this junction was assessed at six locations across the center part of each wound and averaged to determine the average wound depth [Fig. 8(a)]. SFDI scattering values, averaged in the center region for each wound at a single wavelength (658 nm), showed a strong correlation ($r^2 = 0.94$) to measured burn depth for time points greater than 24 h and for all burn severities [Fig. 8(b)]. All time points and burn types for the corresponding recovered burn depths were plotted against A and b. A and b parameters were also strongly correlated ($r^2 = 0.89$ and 0.95 respectively) to burn depth [Fig. 8(b)]. We hypothesized that the differential contrast in scattering in burns was primarily due to the phase changes in tissue collagen. Thermal burns have been previously shown to cause denaturation of collagen, which disrupts the normal structure and distribution of fibrils.[12,40] As shown in Fig. 9, a Masson's trichrome immunostain positively identified the changes in collagen structure for different burn severities, in support of our hypothesis. Normal tissue has a clear basket-weave structure [Fig. 9(a)] in a partial thickness burn [Fig. 9(b)]. In contrast, this basket-weave structure disappears as the tissue is damaged by the burn injury [Fig. 9(c)].

3.4 *Wide-Field Snapshot Imaging of Burn Extent*

A major utility of SFDI is wide-field mapping of both the functional and structural changes in tissue architecture. To demonstrate this utility, we created a wide-field (28 × 10 cm) map of reduced scattering (Fig. 10) for three different severities (superficial, deep partial, and full thickness) and four different time points (2, 24, 48, and 72 h) immediately before the animal was sacrificed. This larger FOV was achieved by stitching together two 15 × 10 cm SFDI images acquired prior to sacrifice. In Fig. 10(a), color images of burns of the same severity appear very different to the eye depending on the age of the burn

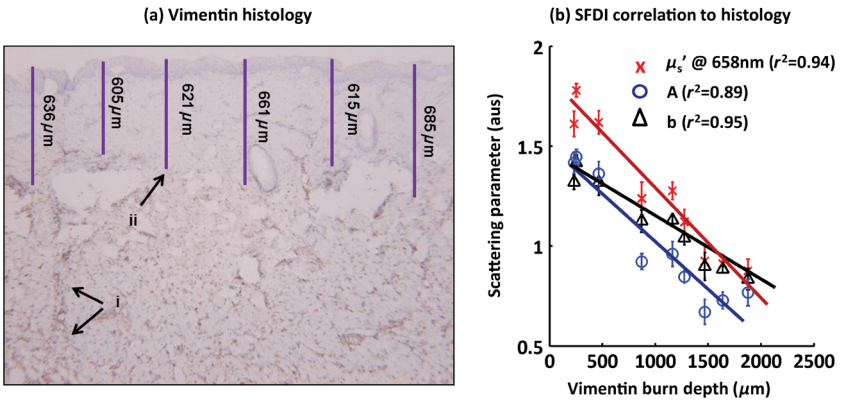

Fig. 8 (a) The burn depth was measured at multiple sites in the center of a superficial partial thickness wound and then averaged. (i) Healthy tissue was identified by positive vimentin stain and burn depth by determining (ii) margin between positive and negative stain. (b) Correlation between histology-based burn depth measurements and SFDI derived scattering signals at a single wavelength shows a strong negative correlation ($r^2 > 0.89$) for all measurements 24 h after injury. The same is true for wavelength-dependent scattering parameters (A, b).

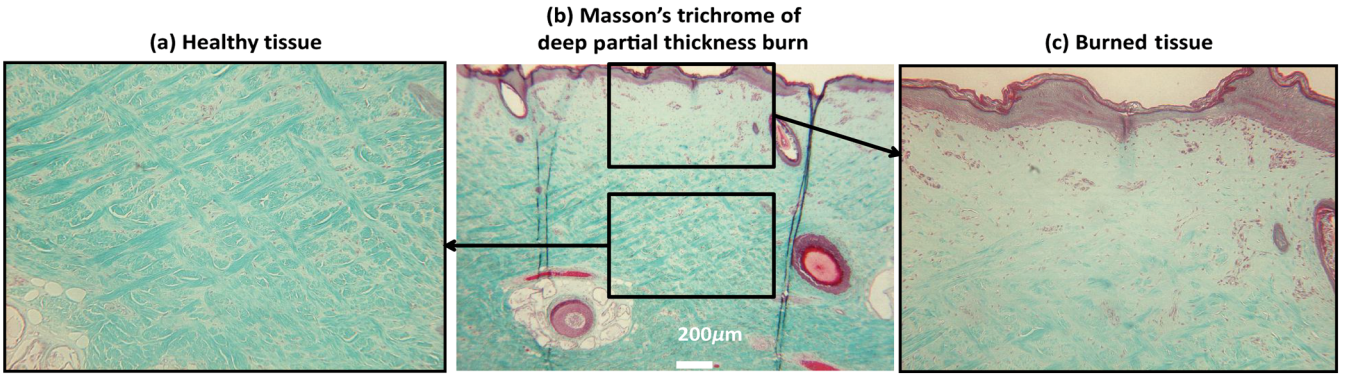

Fig. 9 Representative changes in collagen structure due to a burn injury as seen by Masson's trichrome stain. (a) The classic "basket-weave" pattern disappears as a (b) function of depth due to thermal denaturation depending on severity of burn, (c) burned tissue lacks this structure and appears to be a more homogenous structure.

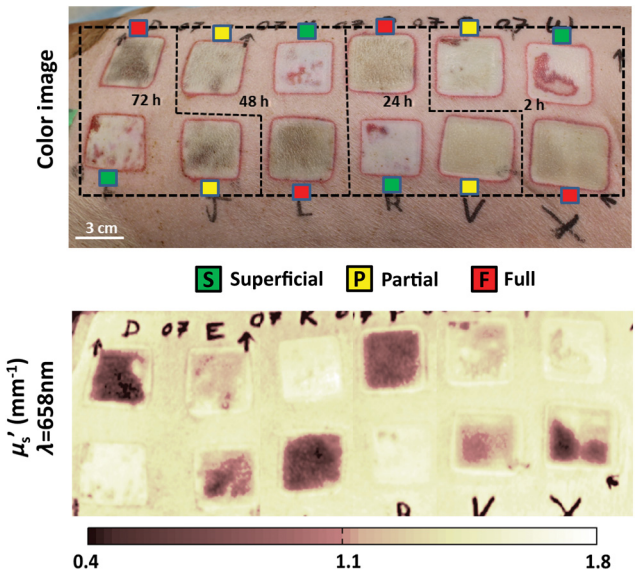

Fig. 10 Overlay of color image and reduced scattering map ($\lambda = 658$ nm) highlights the ability of SFDI to perform snapshot noninvasive wide-field quantitative mapping of burn severity and extent no matter age of the injury.

injury. However, reduced scattering images of the burn appear to separate each burn type independent of the wound age (Fig. 10). The darker areas represent the most severe wounds and are consistent independent of the burn age. This capability highlights the ability to measure a number of wound severities in a single snapshot to characterize the distribution of wound severity.

4 Discussion

In this work, we have presented a wide-field optical imaging technique with the potential to assess burn severity and extent over large surface areas in a noncontact manner (~300 cm^2). First, we presented the multitude of outputs that SFDI can calculate to assess the functional and structural status of the tissue. stO_2 was shown to decrease over the first 72 h for more severe burns due to compromised vasculature networks. Tissue hemoglobin was less sensitive to burn severity, but showed a general increase following all wounds. The gradual progression of the functional status of a wound over the first 72 h highlighted the complex wound healing response postinjury. None of the functional parameters were significantly different between the two most severe burn types. This lack of accurate early discrimination of burn type based on the functional measures alone may be because the blood volume increases in the first 24 to 48 h are

accompanied by concurrent healing inflammatory response and/or blood pooling due to damaged vascular supply, which would also affect the blood volume. The ischemic status of the more severely damaged tissue contributes to the gradual decreases in stO_2 over the first 72 h. This analysis did not explicitly account for absorption by other hemoglobin species, such as methemoglobin or carboxy-hemoglobin, which are known to be associated with burn injury.[41] Based on author's experience, the presence of these heme products tends to result in an overestimation of ctHHb in this with the NIR spectroscopy models employed in this study due to their high absorption in 600 to 700 nm. While accommodating for other hemoglobin products is part of ongoing work, these other products less directly affect the oxy-hemoglobin determination. Thus, both ctHbT and stO_2 parameters are anticipated to be largely unaffected, as they would be somewhat accounted for in the ctHbT parameter (via ctHHb), but not modify ctO_2Hb.

Interestingly, SFDI measures of structural correlates (tissue scattering) appeared to be more sensitive for early measures of burn injury severity compared to that of the functional measures. Superficial thickness burns were easily distinguished from deep partial thickness and full thickness burns immediately after the burn based on the scattering signal ($p < 0.01$). It is plausible that the primary source of this contrast is due to changes in collagen, as the size and distribution of collagen fibrils are the primary contrast mechanism for scattering signals in skin.[36] As shown in the Masson's trichrome histology slides, a thermal insult causes denaturation and effectively melts the collagen fibrils, creating larger aggregates of amorphous collagen. This denaturing observation has been seen using psOCT and SHG microscopy,[12,40] and confirms the idea that significantly burned tissues consist of a distribution of fewer scattering particles with larger scattering cross sections. At a mesoscopic optical level, this translates to a lower A (scattering cross-section) and a lower b (wavelength dependence) value when considering a power-law behavior, Eq. (1), as is commonly used to characterize the tissue scattering spectra. Our analysis of the SFDI-determined scattering spectra is consistent with this finding (A and b both decrease). A fully damaged dermis will have no fibrils intact and exhibit the most dramatic change from normal skin. Thus, it can be argued that SFDI indirectly assesses the density and size of collagen fibrils in the dermis and could potentially provide the basis for wide-field assessment of burn-related dermal damage, a key hallmark to understanding burn depth. This early time point (<24 h) assessment of burn depth has the potential to tremendously impact the standard of care in the burn unit. Decisions to graft or to proceed with wound care can be made earlier than the current 3-day to 1 week standard wait time and can potentially reduce the risk of infections. The objectivity will appropriately stratify patients for appropriate management thereby improving patient outcomes and reducing the length of stay in the hospital.

We have also correlated the mean reduced scattering signal and wavelength-dependent scattering parameters (A and b) to measured burn depth as determined by histology. Compared to microscopic histological sampling, *in vivo* wide-field SFDI measurements of mesoscopic tissue properties (~1 mm lateral resolution with 3 to 4 mm optical depth penetration) are an attractive clinical tool for burn assessment, as burns commonly occur over many cm length scale, often with a strong degree of spatial heterogeneity. This work is one of the few examples of correlating mesoscopic SFDI measures to microscopic functional and structural status, and to the author's knowledge, the first to do this in a porcine model for burns.

This study employed homogenous tissue light transport models to assess depth-averaged absorption and reduced scattering; in the next phase of research, we hope to apply versions of multilayer models to mimic both the skin and burned tissue in order to see if sensitivity to burn severity improves.[42,43] These models may help when dealing with the layers of eschar in burned tissue (if assessing prior to application of hydrotherapy) and may also account for the presence of melanin in normal or mildly burned skin, a common issue for LDI. These layered models could also be helpful in understanding differences in optical signals for different zones of damage (i.e., hyperemia and zone of stasis).

Burn wound evolution over the first week postinjury is expected;[7,44] thus, there is potential for SFDI to follow wound evolution and predict burn outcome at various stages postinjury using a burn index (or indices) derived from SFDI parameters (stO_2, hemoglobin, and scattering). Correlation to outcome was not possible in our current study design, however, as the fate of the deep partial wounds past 72 h is unknown. Ultimately, a link to outcome is expected to have the most clinical impact in terms of guiding treatment plans; therefore, work remains to study SFDI signals past the first few days postinjury.

While the prototype used in these studies was suitable for a controlled preclinical setting, future hardware work will focus on optimization of wavelength and spatial frequency acquisition to improve the overall imaging time. To understand the sources of optical contrast in burn wounds without prejudice, the data in this study were oversampled (extra spatial frequencies, extra wavelengths). Based on our findings in this work, we believe we can readily reduce imaging time to ~1 to 2 s per SFDI dataset. This will eliminate or drastically reduce some of the potential pitfalls for clinical acquisition, including motion artifacts, patient comfort, and sensitivity to ambient light conditions. Applying look-up table inversion approaches and graphics processor unit acceleration can reduce the processing times to the order of acquisition times (~1 s). These advancements will make the realization of an SFDI-based burn imaging system practical for clinical use.

5 Conclusion

We have presented preclinical results demonstrating noncontact assessment of burn severity and extent over large surface areas using an optical imaging platform. Wide-field optical signatures have been correlated to microscopic histological measures of the burn depth. This work lays the ground work for further hardware refinements and algorithm development needed to build an optimized system to scan and assess burned tissues over large surface areas in a clinical setting.

Acknowledgments

This work was supported by a TATRC funded Phase II SBIR (W81XWH11C0108) and NIAMS Phase II SBIR (R44AR064657). The authors would like to acknowledge assistance from Pierre Khoury, Frederick Ayers, and Dr. Anthony Pacifico. *Conflict of Interest*: David Cuccia is co-founder of Modulated Imaging Inc. and holds in equity in the company. Amaan Mazhar and Steve Saggese were full-time employees of Modulated Imaging Inc. at the time of the study.

References

1. M. D. Peck, "Epidemiology of burns throughout the world. Part I: distribution and risk factors," *Burns* **37**(7), 1087–1100 (2011).
2. American Burn Association, "2013 national burn repository. Report of data from 2003–2012," in *Proc. American Burn Association*, American Burn Association, Chicago, Illinois (2013).
3. D. M. Heimbach et al., "Burn depth estimation—man or machine," *J. Trauma* **24**(5), 373–378 (1984).
4. D. Heimbach et al., "Burn depth: a review," *World J. Surg.* **16**(1), 10–15 (1992).
5. A. M. Watts et al., "Burn depth and its histological measurement," *Burns* **27**(2), 154–160 (2001).
6. A. D. Jaskille et al., "Critical review of burn depth assessment techniques: Part I. Historical review," *J. Burn Care Res.* **30**(6), 937–947 (2009).
7. L. B. Nanney, B. A. Wenczak, and J. B. Lynch, "Progressive burn injury documented with vimentin immunostaining," *J. Burn Care Rehabil.* **17**(3), 191–198 (1996).
8. M. A. Afromowitz et al., "Multispectral imaging of burn wounds: a new clinical instrument for evaluating burn depth," *IEEE Trans. Biomed. Eng.* **35**(10), 842–850 (1988).
9. K. S. Black et al., "Burn depth evaluation with fluorometry: is it really definitive?," *J. Burn Care Rehabil.* **7**(4), 313–317 (1986).
10. J. M. Still et al., "Diagnosis of burn depth using laser-induced indocyanine green fluorescence: a preliminary clinical trial," *Burns* **27**(4), 364–371 (2001).
11. M. H. Arbab et al., "Terahertz spectroscopy for the assessment of burn injuries in vivo," *J. Biomed. Opt.* **18**(7), 077004 (2013).
12. M. C. Pierce et al., "Collagen denaturation can be quantified in burned human skin using polarization-sensitive optical coherence tomography," *Burns* **30**(6), 511–517 (2004).
13. K. H. Kim et al., "In vivo imaging of human burn injuries with polarization-sensitive optical coherence tomography," *J. Biomed. Opt.* **17**(6), 066012 (2012).
14. N. Iftimia et al., "Combined reflectance confocal microscopy/optical coherence tomography imaging for skin burn assessment," *Biomed. Opt. Express* **4**(5), 680–695 (2013).
15. M. Kaiser et al., "Noninvasive assessment of burn wound severity using optical technology: a review of current and future modalities," *Burns* **37**(3), 377–386 (2011).
16. A. D. Jaskille et al., "Critical review of burn depth assessment techniques: part II. Review of laser Doppler technology," *J. Burn Care Res.* **31**(1), 151–157 (2010).
17. S. Monstrey et al., "Assessment of burn depth and burn wound healing potential," *Burns* **34**(6), 761–769 (2008).
18. L. H. Kim et al., "The impact of laser Doppler imaging on time to grafting decisions in pediatric burns," *J. Burn Care Res.* **31**(2), 328–332 (2010).
19. C. J. Stewart et al., "A comparison of two laser-based methods for determination of burn scar perfusion: laser Doppler versus laser speckle imaging," *Burns* **31**(6), 744–752 (2005).
20. A. Bednov et al., "Correlation properties of multiple scattered light: implication to coherent diagnostics of burned skin," *J. Biomed. Opt.* **9**(2), 347–352 (2004).
21. K. M. Cross et al., "Clinical utilization of near-infrared spectroscopy devices for burn depth assessment," *Wound Repair Regen.* **15**(3), 332–340 (2007).
22. M. G. Sowa et al., "Classification of burn injuries using near-infrared spectroscopy," *J. Biomed. Opt.* **11**(5), 054002 (2006).
23. D. J. Cuccia et al., "Quantitation and mapping of tissue optical properties using modulated imaging," *J. Biomed. Opt.* **14**(2), 024012 (2009).
24. D. J. Cuccia et al., "Modulated imaging: quantitative analysis and tomography of turbid media in the spatial-frequency domain," *Opt. Lett.* **30**(11), 1354–1356 (2005).
25. S. Gioux et al., "First-in-human pilot study of a spatial frequency domain oxygenation imaging system," *J. Biomed. Opt.* **16**(8), 086015 (2011).
26. A. Ponticorvo et al., "Quantitative assessment of partial vascular occlusions in a swine pedicle flap model using spatial frequency domain imaging," *Biomed. Opt. Express* **4**(2), 298–306 (2013).
27. A. Yafi et al., "Postoperative quantitative assessment of reconstructive tissue status in a cutaneous flap model using spatial frequency domain imaging," *Plastic Reconstr. Surg.* **127**(1), 117–130 (2011).
28. A. Mazhar et al., "Spatial frequency domain imaging of port wine stain biochemical composition in response to laser therapy: a pilot study," *Lasers Surg. Med.* **44**(8), 611–621 (2012).
29. A. M. Laughney et al., "Spectral discrimination of breast pathologies in situ using spatial frequency domain imaging," *Breast Cancer Res.* **15**(4), R61 (2013).
30. J. Q. Nguyen et al., "Spatial frequency domain imaging of burn wounds in a preclinical model of graded burn severity," *J. Biomed. Opt.* **18**(6), 066010 (2013).
31. T. T. Nguyen et al., "Novel application of a spatial frequency domain imaging system to determine signature spectral differences between infected and noninfected burn wounds," *J. Burn Care Res.* **34**(1), 44–50 (2013).
32. T. A. Erickson et al., "Lookup-table method for imaging optical properties with structured illumination beyond the diffusion theory regime," *J. Biomed. Opt.* **15**(3), 036013 (2010).
33. S. Gioux et al., "Three-dimensional surface profile intensity correction for spatially modulated imaging," *J. Biomed. Opt.* **14**(3), 034045 (2009).
34. A. Mazhar et al., "Wavelength optimization for rapid chromophore mapping using spatial frequency domain imaging," *J. Biomed. Opt.* **15**(6), 061716 (2010).
35. J. R. Mourant et al., "Predictions and measurements of scattering and absorption over broad wavelength ranges in tissue phantoms," *Appl. Opt.* **36**(4), 949–957 (1997).
36. S. L. Jacques, "Optical properties of biological tissues: a review," *Phys. Med. Biol.* **58**(11), R37–R61 (2013).
37. P. Ganapathy et al., "Dual-imaging system for burn depth diagnosis," *Burns* **40**(1), 67–81 (2014).
38. R. Bott et al., "A silicone-based controlled-release device for accelerated proteolytic debridement of wounds," *Wound Repair Regen.* **15**(2), 227–235 (2007).
39. N. Kollias et al., "Endogenous skin fluorescence includes bands that may serve as quantitative markers of aging and photoaging," *J. Invest. Dermatol.* **111**(5), 776–780 (1998).
40. R. Tanaka et al., "In vivo visualization of dermal collagen fiber in skin burn by collagen-sensitive second-harmonic-generation microscopy," *J. Biomed. Opt.* **18**(6), 061231 (2013).
41. E. Wolak et al., "Methemoglobinemia in critically ill burned patients," *Am. J. Crit. Care* **14**(2), 104–108 (2005).
42. D. Yudovsky and A. J. Durkin, "Spatial frequency domain spectroscopy of two layer media," *J. Biomed. Opt.* **16**(10), 107005 (2011).
43. D. J. Cuccia, *Models, Instrumentation, and Applications for Spatial Frequency Domain Imaging*, OSA Biomed, Miami, Florida (2014).
44. C. L. Riordan et al., "Noncontact laser Doppler imaging in burn depth analysis of the extremities," *J. Burn Care Rehabil.* **24**(4), 177–186 (2003).

Amaan Mazhar is the director of research and development at Modulated Imaging Inc. He received his PhD degree from the Beckman Laser Institute at the University of California, Irvine, in 2010, and focused on SFDI related research. He has co-authored 20 publications, book chapters, and patent applications in the field of biomedical optics since 2007.

Steve Saggese has over 20 years of experience on the research, design, and development of optical imaging systems for medical, military and commercial applications. He has held a variety of positions in technical and management roles. For medical devices, he has led and supported the design and fabrication of multiple imaging systems for the evaluation of tissue health for use in wound analysis, burn assessment, and photodynamic therapy dose optimization.

Alonda C. Pollins is a senior research specialist in plastic surgery at Vanderbilt's School of Medicine. She received her BS degree in 2001 and Master of Laboratory Investigation in 2006. She has worked in research for 15 years, 12 of that in the plastic surgery lab at Vanderbilt, and has co-authored 12 manuscripts. Her primary work is with cutaneous wound healing, with extensive experience in the porcine model.

Nancy L. Cardwell is the Laboratory Manager for the Plastic Surgery Research Laboratory in Vanderbilt's School of Medicine. She has a Bachelor of Science degree with a minor in animal science from Middle Tennessee State University. She has worked in the research setting at Vanderbilt University Medical Center since 1986.

Lillian Nanney is a professor of plastic surgery, cell and developmental biology at Vanderbilt's School of Medicine, and she is the author of 175 manuscripts on chronic and acute wound healing. She is a former president of the Wound Healing Society and has a long-standing interest in burn depth progression and the acute burn wound. She is well known for her work with porcine modules of cutaneous injury.

David J. Cuccia is a cofounder of Modulated Imaging Inc. and the current CEO/CTO. He received his PhD degree from the Beckman Laser Institute at the University of California, Irvine, in 2006. He was the lead author on seminal publications describing SFDI and has coauthored 37 publications, patents, and book chapters in the field of biomedical optics since 2006. He is also the PI on the grant that funded this research.